Progress In Electromagnetics Research Letters, Vol. 111, 35–43, 2023

A Miniaturized Frequency Selective Rasorber with High Frequency Harmonic Suppression

Lei Deng, Shixing Yu, and Na Kou*

Abstract—A frequency selective absorber for harmonic absorption (HA-FSR) is proposed in this paper. It consists of a miniaturized frequency selective surface (FSS) for harmonic suppression and a circuit analog absorber (CAA) for harmonic absorption. The frequency selective rasorber (FSR) unit is 6.7 mm × 6.7 mm ($0.129\lambda \times 0.129\lambda$, where λ is the free space wavelength of 5.8 GHz). The simulation and measurement show that the HA-FSR can generate a transmission band from 4.51 GHz to 7.47 GHz and a −10 dB absorption band from 11.96 GHz to 22.31 GHz, which covers more than 3 times of the main passband harmonic band. In addition, the FSR has good polarization stability and angle stability within 30° of oblique incidences under both TE and TM polarizations, which can be applied to electromagnetic interference shielding field and low-observable platforms.

1. INTRODUCTION

Fransis Hopkinson first proposed the frequency selective surface (FSS) theory in the 18th century [1]. So far, various filtering performance FSSs have been studied, such as broadband filtering response FSS [2, 3] and multi-band filtering response FSS [4, 5]. Generally, FSS is a periodic array composed of resonant or non-resonant elements. For bandpass FSS, in addition to the transmission passband of resonant frequency points, the transmission passband will also appear in high frequency harmonic band. As a result, the communication system will be subjected to serious electromagnetic interference, and the radar cross-section (RCS) value will increase, which is not conducive to the stealth of the system. In order to reduce the spurious transmission influence of FSS on a radar system at harmonic bands, FSS [6–8] with harmonic suppression effect needs to be considered. However, the harmonic suppressed FSS acts as the full reflection at high frequency harmonic bands, which leads to the loss of stealth performance of FSS under enemy multi-station radar detection system. Frequency selective rasorber (FSR) can effectively absorb the reflected waves outside the transmission passband, reduce the RCS value, and improve the stealth performance. In most cases, FSR is a combination of a circuit analog absorber (CAA) [9, 10] and an FSS, which has the characteristics of in-band transmission and out-of-band absorption [11–13]. If a CAA with harmonic absorption is combined with an FSS of harmonic suppression, an FSR with high frequency harmonic absorption can be designed [14, 15]. This kind of FSR not only absorbs the high frequency harmonic reflection wave, reduces the RCS value, improves the stealth and anti-interference ability of the wireless communication system, but also guarantees the transmission performance of FSS with low loss.

In [14], a harmonic suppression FSR based on a square ring resonator FSS and high-impedance surface (HIS) was reported, but its absorption performance in high frequency harmonic band under oblique incidence was not optimal. In [15], a harmonic-suppression frequency selective rasorber (HS-FSR) design based on a non-resonant FSS and square resistance film is reported to achieve stable

Received 24 April 2023, Accepted 12 June 2023, Scheduled 20 June 2023

* Corresponding author: Na Kou (nkou@gzu.edu.cn).

The authors are with the Key Laboratory of Micro-Nano-Electronics and Software Technology of Guizhou Province, College of Big Data and Information Engineering, Guizhou University, Guiyang 550025, China.

absorption properties across two to three harmonics in the main passband. However, the FSS structure consists of inductive square loops and capacitive patches coupled with each other, and the overall structure is large. In this paper, we design a miniaturized second-order FSS with harmonic suppression characteristics using resonant elements, which can generate transmission passband and achieve full reflection suppression of high frequency harmonics. Then a high frequency absorption CAA is used to realize the absorption characteristics of high frequency harmonics and complete the design of the frequency selection of harmonic absorption absorber (HA-FSR). Simulation and measurement results show that the HS-FSR can generate a passband with a -3 dB bandwidth of 52.1% from 4.42 to 7.53 GHz. From 11.21 GHz to 22.87 GHz, the absorbtivity with more than 80% can be obtained, and the relative bandwidth is 67.4%, covering more than 3 times of the main passband harmonic frequency band. In addition, the FSR has good polarization stability and angle stability within 30° of oblique incidences under both TE and TM polarizations. It can have application prospect in the field of electromagnetic interference shielding and stealth radome.

2. TOPOLOGY AND EQUIVALENT CIRCUIT MODEL OF FSR

The proposed FSR consists of a miniaturized circuit analog absorber and a harmonic suppressed FSS. F4B with a relative dielectric constant of 2.65, tangent loss of 0.001, and thickness of 0.5 mm is selected as the dielectric substrate for the absorber. FR-4, whose relative dielectric constant is 4.4, and tangent loss is 0.02, is selected as the plate for FSS with harmonic suppression. The proposed FSR topology is shown in Figure 1. The top layer is a broadband absorber loaded with lumped resistors, and the middle and lower layers are harmonic suppression FSS. In order to understand the working principle of the proposed FSR, the equivalent circuit analysis of the structure is carried out.

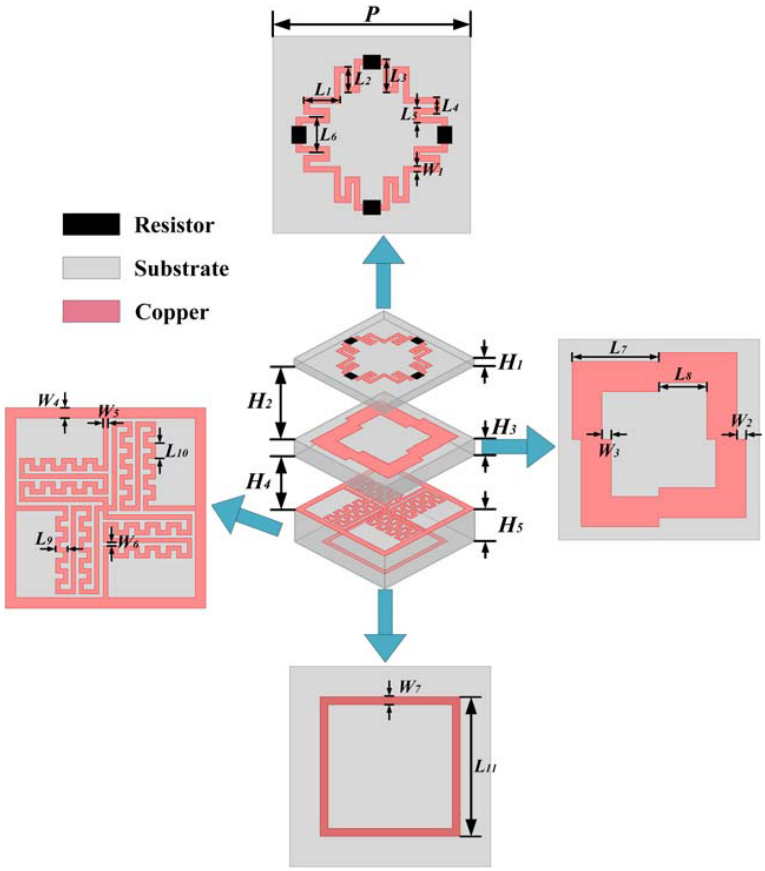

Figure 1. Topology of the proposed FSR.

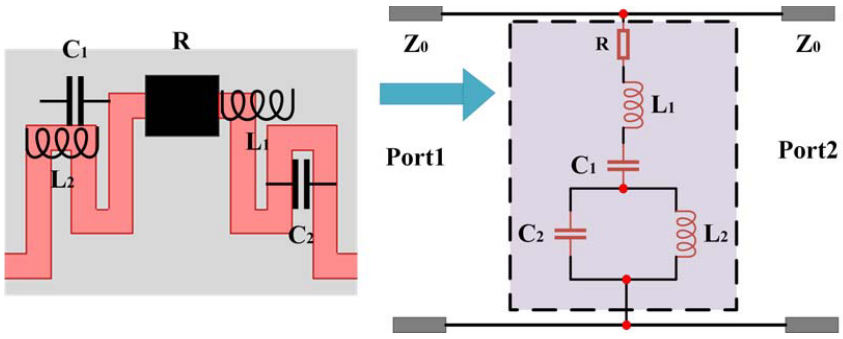

Figure 2. Equivalent circuit model of the absorber.

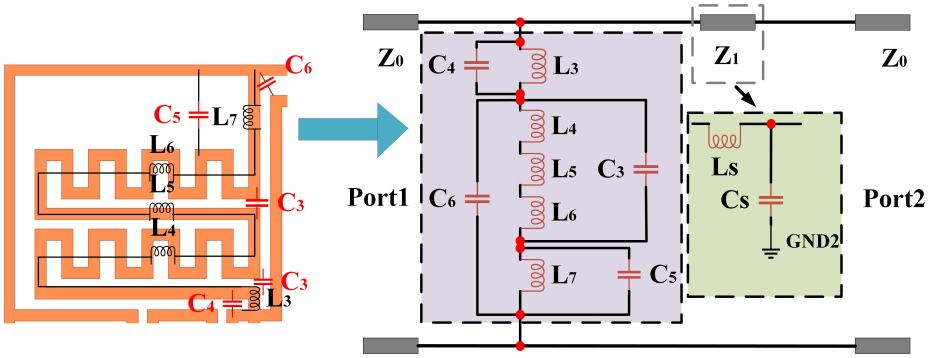

Figure 3. Equivalent circuit model of the DCGF structure.

The equivalent circuit of the absorbing structure is shown in Figure 2, where R represents the lumped resistor, and inductor L_1 is realized by a metal strip parallel to the direction of the electric field. Capacitor C_1 is constructed by the gap between adjacent units. Inductor L_2 and capacitor C_2 are realized by bending metal strips and gaps between them, respectively.

The harmonic suppressed FSS is designed by cascading a mutated square ring and band-pass FSS, wherein the band-pass FSS consists of two layers of metal etched on the same dielectric substrate. The upper metal layer is a double comb grids structure (DCGF) with metal fence, and the lower metal one is a resonant square ring. According to the rotation symmetry of the DCGF structure, only the equivalent circuit of the DCGF 1/4 part is analyzed. As shown in Figure 3, inductor L_3 can be generated by the short line; Inductors L_4 and L_6 can be derived from two comb grids, respectively. In addition, L_5 can be equivalent to the metal strip between two comb grids; L_7 can be produced by a metal strip attached to the metal fence. L_3 affects the frequency of the second passband, and the smaller the value is, the higher the passband range is. L_4, L_5, and L_6 determine the frequency of the first passband, and the higher the inductance values are, the lower the frequency range is. Capacitors C_3, C_4, C_5, and C_6 can be equivalent to the couplings between two different metal strips or comb grids, respectively. C_3 determines the position of the first passband. The larger the value of C_3 is, the lower range of the passband is. C_4, similar to L_3, affects the frequency of the second passband. The smaller the value of C_4 is, the higher range of the second passband is. Finally, the corresponding equivalent circuit can be constructed, as shown in Figure 3. Z_0 is the free space impedance, and Z_1 is the impedance of dielectric substrate in which its equivalent inductance and capacitance can be expressed as: $Ls = \mu_0\mu_r h$, $Cs = \varepsilon_0\mu_r h/2$. Figure 4 shows the transmission coefficient comparison between circuit analysis and full-wave simulation. We can see that the two results agree well with each other.

Finally, we can obtain the equivalent circuit model of FSR, as shown in Figure 5. Zs is the characteristic impedance of harmonic suppression FSS, and Za is the characteristic impedance of the absorber. The equivalent circuit analysis illustrated in the manuscript is used to roughly deduce the frequency response of the proposed FSR structure. We only provide how the equivalent lumped elements

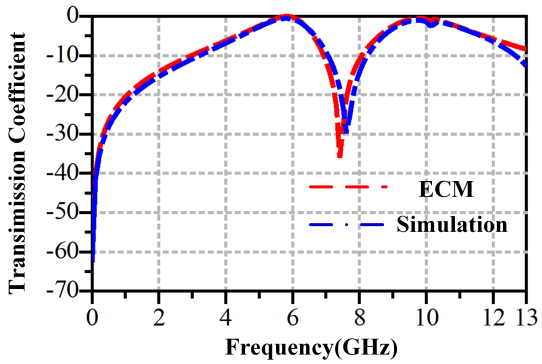

Figure 4. The transmission coefficient comparison between circuit analysis and full-wave simulation.

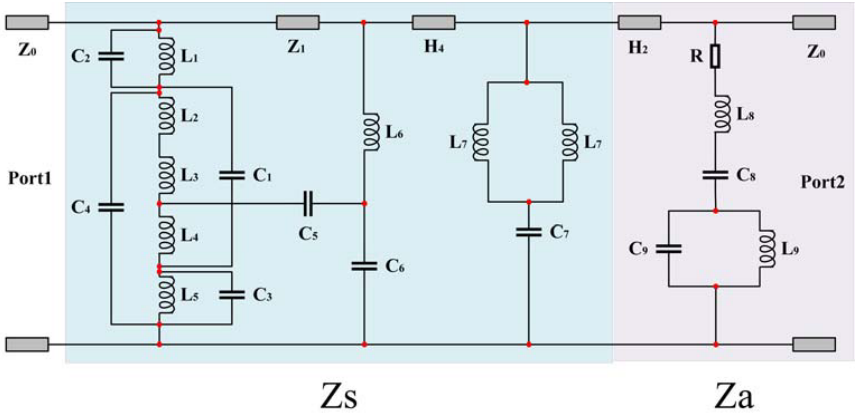

Figure 5. Equivalent circuit model of FSR.

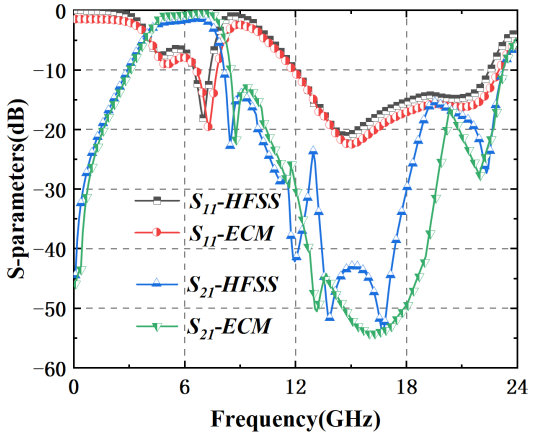

Figure 6. Comparison of S parameters between circuit analysis and full-wave simulation.

changes with variation of physical parameters of an FSR structure but not analytical formulas since the complexity of FSR structure is high. Table 1 shows the equivalent lumped parameter values of circuit. The circuit analyzed results are compared with the full-wave simulation results, as shown in Figure 6. It can be seen that the equivalent circuit model (ECM) calculation results are consistent with the full-wave simulation results, which proves the authenticity of the design.

Table 1. Equivalent circuit parameters.

L_1	L_2	L_3	L_4	L_5	C_1	C_2	C_3	C_4	C_5
0.85 nH	0.69 nH	0.67 nH	0.5 nH	0.03 nH	0.42 pF	0.32 pF	8.08 pF	0.01 pF	0.01 pF
L_6	C_6	L_7	C_7	R	L_9	L_{10}	C_8	C_9	
0.3 nH	0.02 pF	2.8 nH	0.06 pF	200	10.6 nH	4.8 nH	0.02 pF	0.1 pF	

3. PERFORMANCES ANALYSES

The FSR structure is simulated by using the master-slave boundary conditions which is used to perform the periodic boundary conditions (PBCs) for modeling infinite frequency selective rasorber, and two Floquet excitation ports with two perpendicular excitation electric fields on the top and bottom of FSR are added to analyze the transmission characteristics of the unit cell under different polarizations (TE and TM polarizations), as shown in Figure 7. Figure 8 shows the simulated transmission coefficient, reflection coefficient, and absorbtivity of proposed FSR under oblique incidence TE and TM polarizations. We can see that the passbands of the FSR under two polarizations both range from 4.51 GHz to 7.47 GHz. With the increase of incident angle, the passband range and insertion loss under the two polarizations remain almost unchanged. Under normal incidence, the passband range for TE polarization is 4.29–7.58 GHz with the −3 dB bandwidth of 55.4%. The absorption band (absorbtivity $\geq$ 80%) is 11.21–22.92 GHz with the relative bandwidth of 68.6%. The passband under TM polarization is 4.42–7.53 GHz, which basically coincides with that under TE polarization. The absorption band ranges from 11.08 GHz to 22.87 GHz, and the relative bandwidth is 69.5%. With the increase of incident angle, the absorption performance of TE polarization is more stable than that of TM polarization. When the incident angle increases to 30°, the absorption performance of TM polarization deteriorates at 18 GHz, but the transmission coefficient and reflection coefficient remain below −10 dB, and the absorbitivity is also greater than 80%.

To verify the performance of the proposed FSR, a prototype consisting of 32×32 units was fabricated and assembled, as shown in Figure 9. It consists of 4 metal layers, 3 dielectric substrates, and patch resistors in 0402 package size. The size of the fabricated FSR is 240 × 240 × 7.3 mm, and it is assembled with plastic screws. Since the frequency band of concern is between 2 GHz and 24 GHz, a pair of

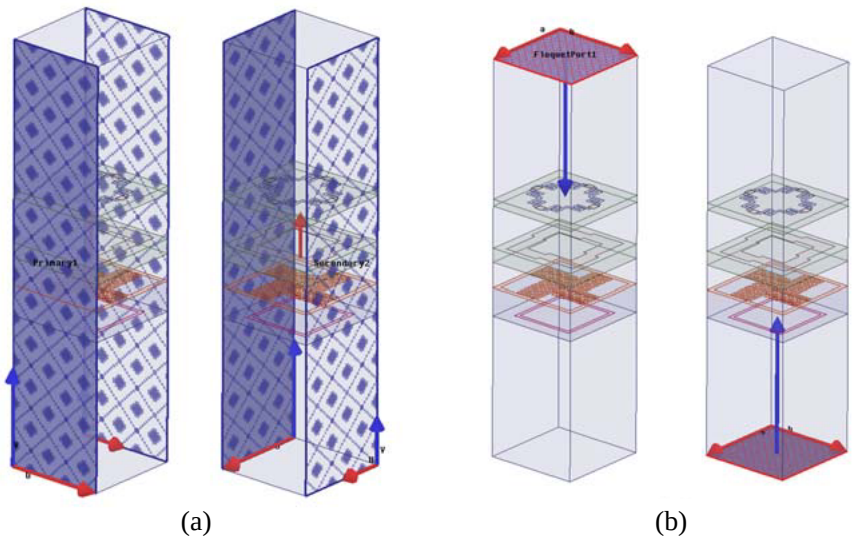

Figure 7. Simulation condition setting. (a) The master-slave boundary conditions. (b) Floquet excitation ports.

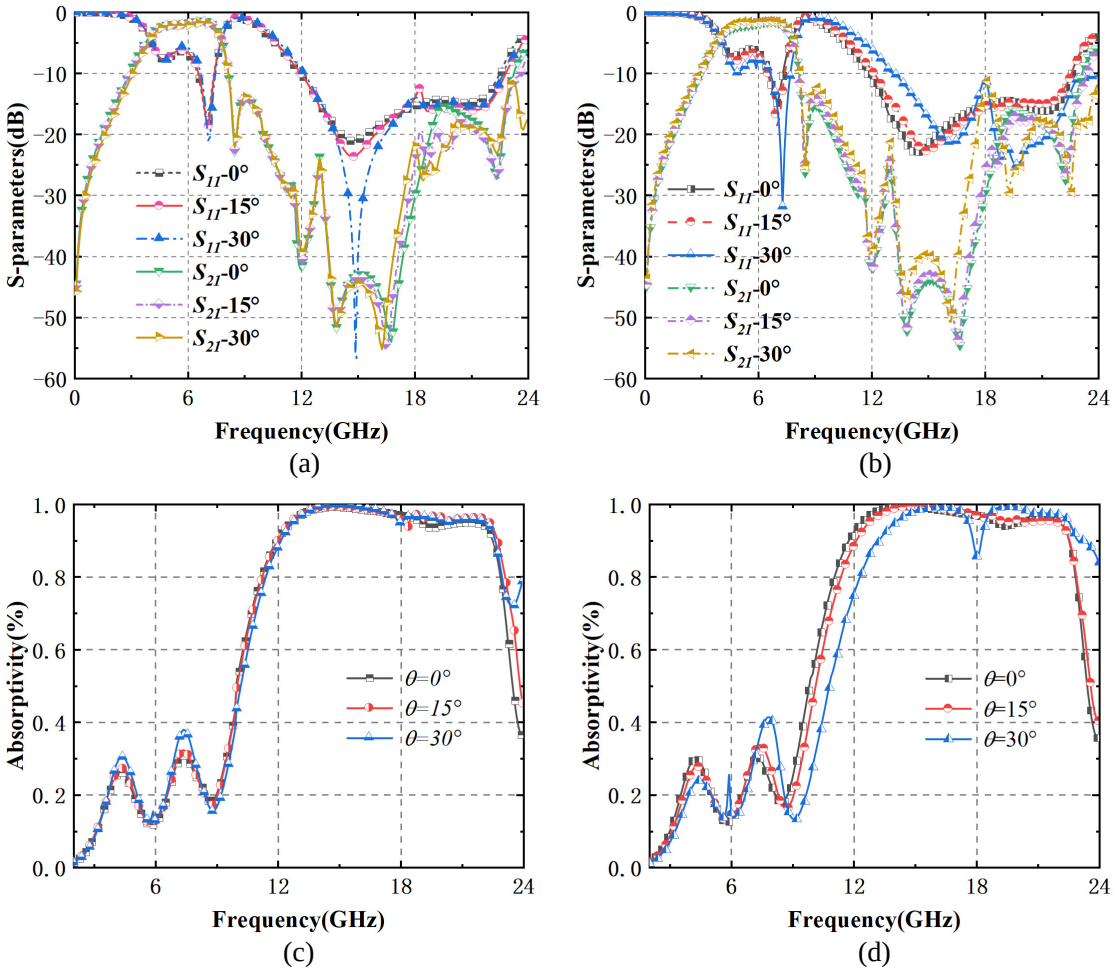

Figure 8. Simulation results of S parameter and absorbitivity curve under oblique incidence. (a), (c) TE mode; (b), (d) TM mode.

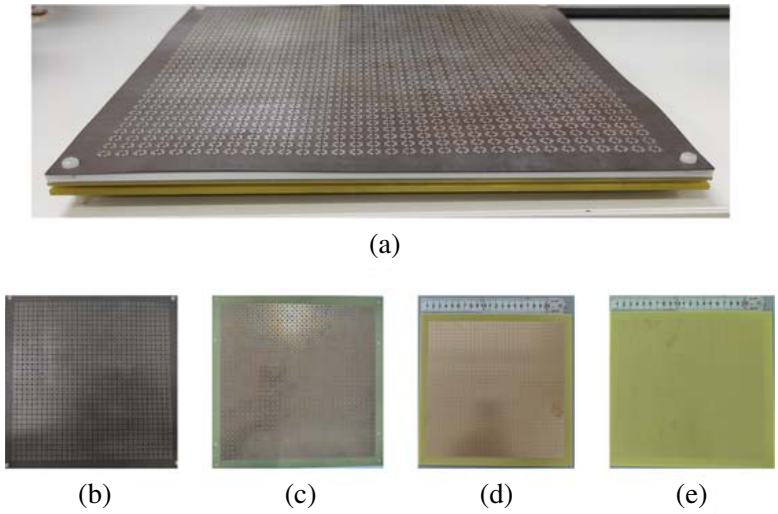

Figure 9. Geometric structure of sample FSR. (a) Three-dimensional graph. (b) Absorbing structure. (c) Ring of variation square. (d) DCGF. (e) Resonant square ring.

wideband horn antennas is used as the transmitting and receiving antennas of the experiment, and their working frequency band is from 2 GHz to 26.5 GHz. The measurement is carried out in an anechoic chamber. The measurement configurations of transmission coefficient (S_{21}) and reflection coefficient (S_{11}) of FSR are shown in Figure 10.

Figure 11 shows the measured transmission and reflection coefficients of the proposed FSR under oblique incidences of TE and TM polarizations. It can be seen that the measured results of the passband are in good agreement with the simulated ones. However, due to the introduction of a new inductance into the welding resistance, the measured $|S_{11}|$ moves up to near -10 dB, but the overall performance

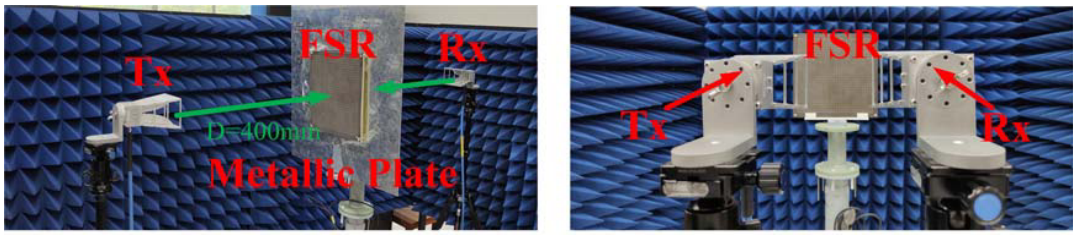

(a) (b)

Figure 10. Measurement configurations for (a) transmission coefficient and, (b) reflection coefficient of FSR.

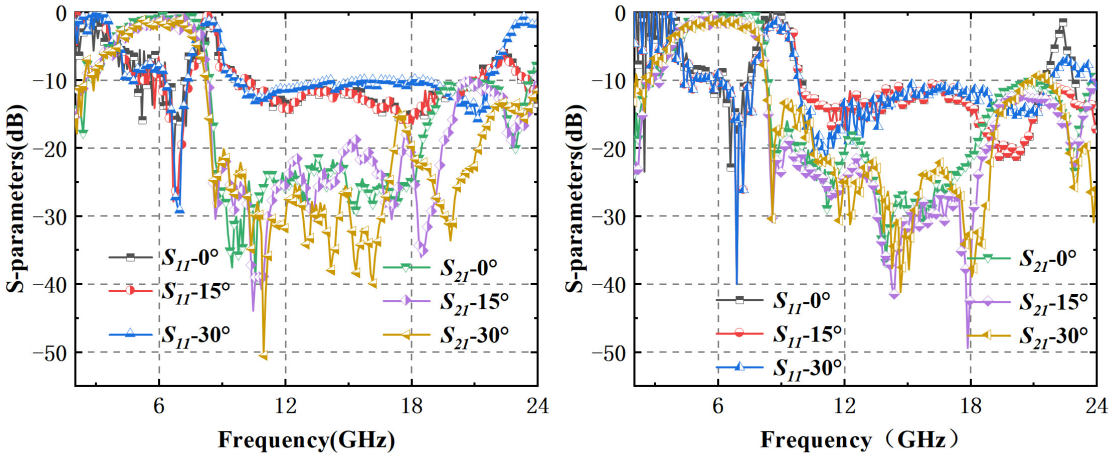

(a) (b)

Figure 11. Measured S_{21} and S_{11} under oblique incidences with (a) TE and, (b) TM polarizations.

Table 2. Performances comparison.

Ref.	f_0/IL[1]	Absorption bandwidth Absorptivity	HS^2 BW^3 of FSS ($S_{21} < -10$ dB)	*Pol.*[4]	*Mea.*[5]
[14]	8 GHz/2 dB	12–26 GHz/> 6 dB	22.5–30 GHz ($\theta = 0°$)	Dual	Yes
[16]	4.65 GHz/1 dB	5.5–12.3 GHz/> 10 dB	5.5–12.3 GHz ($\theta = 0°$)	Single	Yes
[17]	5 GHz/1.5 dB	8.5–11.7 GHz/10 dB	8–12 GHz ($\theta \leq 40°$)	Dual	N.A.
This Work	5.99 GHz/1.78 dB	11.96–22.31 GHz/10 dB	8.15–23.13 GHz ($\theta \leq 30°$)	Dual	Yes

[1]IL=Insertion Loss. [2]HS=Harmonic Suppressed. [3]BW=Bandwidth.
[4]Pol.=Polarization. [5]Mea.=Measurement.

remains in good agreement with the simulation. This further verifies that the proposed FSR can generate the desired passband and harmonic absorption band with good angle and polarization stabilities. Finally, we compare our work with some relevant researches, as shown in Table 2. We can see that our work can effectively realize polarization insensitive harmonic absorption performance which can be used for enhancing the stealth performance of radar systems.

4. CONCLUSION

In this paper, we propose a miniaturized FSR for high frequency harmonic suppression. The equivalent circuit is analyzed, and the sample is processed for verification. The simulation and measurement results show that the main passband of the FSR is 4.51–7.47 GHz, and the bandwidth is close to 3 GHz. Moreover, the harmonic absorption characteristics occur at 11.96–22.31 GHz, covering the main passband by about 3 octaves. The proposed high frequency harmonic suppression FSR can be applied to radome to improve the anti-jamming performance of wireless communication system and stealth performance of radar platform.

ACKNOWLEDGMENT

This work was supported by the National Natural Science Foundation of China under Grant No. 61961006 and the Science and Technology Foundation of Guizhou Province under Grant No. QKHJC [2020]1Y257.

REFERENCES

1. Hopkinson, F. and D. Rittenhouse, "An optical problem, proposed by Mr. Hopkinson, and solved by Mr. Rittenhouse," *Transactions of the American Philosophical Society*, Vol. 2, 201–206, 1786.
2. Sampath, S. S. and R. Sivasamy, "A single-layer UWB frequency-selective surface with band-stop response," *IEEE Transactions on Electromagnetic Compatibility*, Vol. 62, No. 1, 276–279, Feb. 2020.
3. Littman, N. M., S. G. O'keefe, A. Galehdar, H. G. Espinosa, and D. V. Thiel, "Ultra-thin broadband transmission FSS for linear polarization rotation," *IEEE Access*, Vol. 9, 127335–127342, 2021.
4. Yan, M., S. Qu, J. Wang, et al., "A miniaturized dual-band FSS with second-order response and large band separation," *IEEE Antennas and Wireless Propagation Letters*, Vol. 14, 1602–1605, 2015.
5. Suresh Kumar, T. R. and K. J. Vinoy, "Tri-band band-stop frequency selective surface using tortuous Jerusalem cross with angularly stable response," *IEEE Indian Conference on Antennas and Propogation*, 1–4, 2018.
6. Xu, S., Y. Li, M. Ahmed, et al., "A novel miniaturized ultra-wideband frequency selective surface with rapid band edge," *IEEE Access*, Vol. 9, 161854–161861, 2021.
7. Hong, T., M. Wang, K. Peng, Q. Zhao, and S. Gong, "Compact ultra-wide band frequency selective surface with high selectivity," *IEEE Transactions on Antennas and Propagation*, Vol. 68, No. 7, 5724–5729, Jul. 2020.
8. Yu, Z. Y., W. C. Tang, Y. H. Li, and J. P. Zhu, "Highly-selective, closely-spaced, tri-band bandpass three-dimensional frequency selective surface," *IEICE Electronics Express*, Vol. 17, No. 13, 20200153, 2020.
9. Yu, W., G. Q. Luo, Y. Yu, et al., "Dual-polarized band-absorptive frequency selective rasorber using meander-line and lumped resistors," *IEEE Transactions on Antennas and Propagation*, Vol. 67, No. 2, 1318–1322, Feb. 2019.
10. Guo, M., Q. Chen, D. Sang, Y. Zheng, and Y. Fu, "Dual-polarized dual-band frequency selective rasorber with low insertion loss," *IEEE Antennas and Wireless Propagation Letters*, Vol. 19, No. 1, 148–152, Jan. 2020.

11. Omar, A. A., Z. Shen, and H. Huang, "Absorptive frequency-selective reflection and transmission structures," *IEEE Transactions on Antennas and Propagation*, Vol. 65, No. 11, 6173–6178, Nov. 2017.
12. Shen, Z., J. Wang, and B. Li, "3-D frequency selective rasorber: Concept, analysis, and design," *IEEE Transactions on Microwave Theory and Techniques*, Vol. 64, No. 10, 3087–3096, Oct. 2016.
13. Wang, Z. F., J. H. Fu, Q. S. Zeng, M. X. Song, and T. A. Denidni, "Wide-band transmissive frequency-selective absorber," *IEEE Antennas and Wireless Propagation Letters*, Vol. 18, No. 7, 1443–1447, 2019.
14. Yu, S., N. Kou, Z. Ding, and Z. Zhang, "Harmonic-suppressed frequency selective rasorber using resistive-film sheet and square-loops resonator," *IEEE Antennas and Wireless Propagation Letters*, Vol. 19, No. 2, 292–296, Feb. 2020.
15. Yu, S., N. Kou, Z. Ding, and Z. Zhang, "Harmonic-absorption frequency selective rasorber based on non-resonant FSS and resistive-sheet," *IEEE Transactions on Microwave Theory and Techniques*, Vol. 69, No. 8, 3737–3745, Aug. 2021.
16. Omar, A. A., Z. Shen, and H. Huang, "Absorptive frequency-selective reflection and transmission structures," *IEEE Transactions on Antennas and Propagation*, Vol. 65, No. 11, 6173–6178, Nov. 2017.
17. Hamid, S., H. Shakhtour, and D. Heberling, "Frequency selective radome with enhanced transmissive and absorptive response," *Proc. Loughborough Antennas Propag. Conf. (LAPC)*, 36–39, Nov. 2014.